

## SUPPLEMENTARY INFORMATION

### **The impact of antimicrobials on gonococcal evolution**

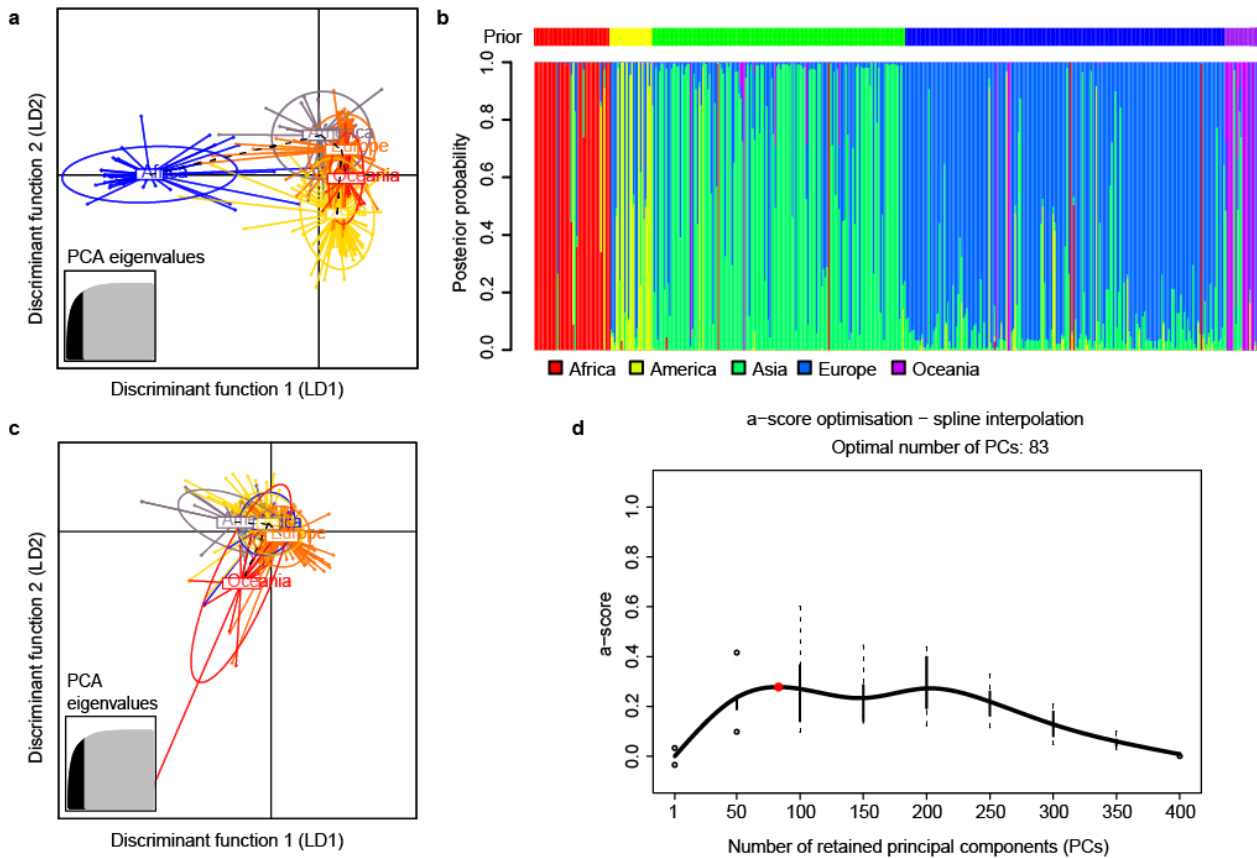
Leonor Sánchez-Busó, Daniel Golparian, Jukka Corander, Yonatan H. Grad, Makoto Ohnishi, Rebecca Flemming, Julian Parkhill, Stephen D. Bentley, Magnus Unemo, Simon R. Harris

This document contains:

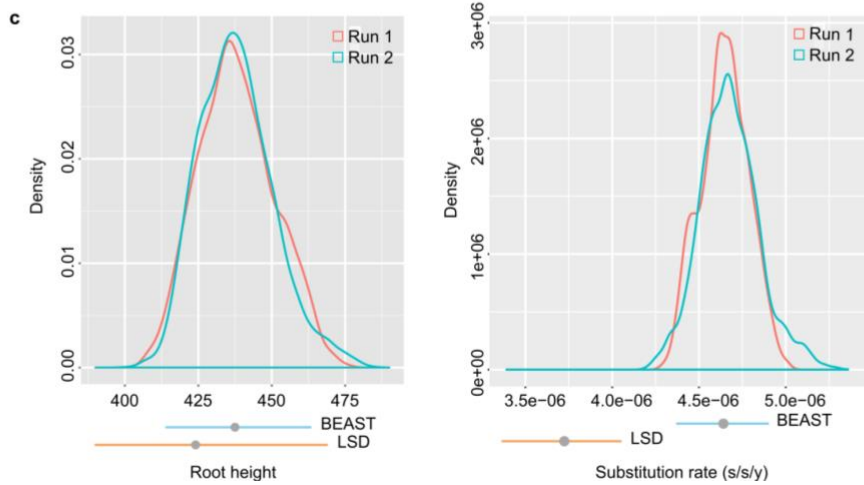
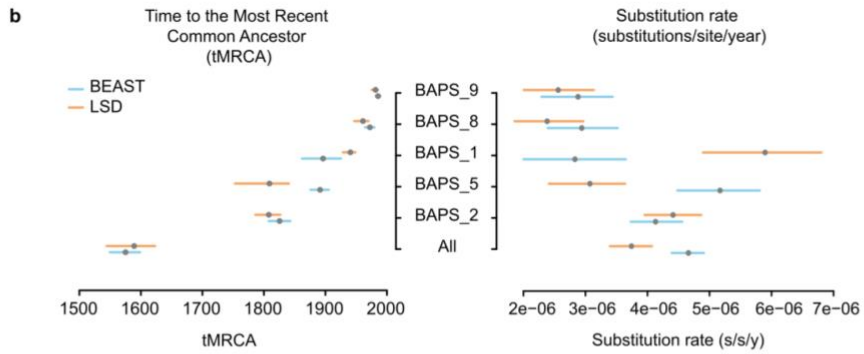
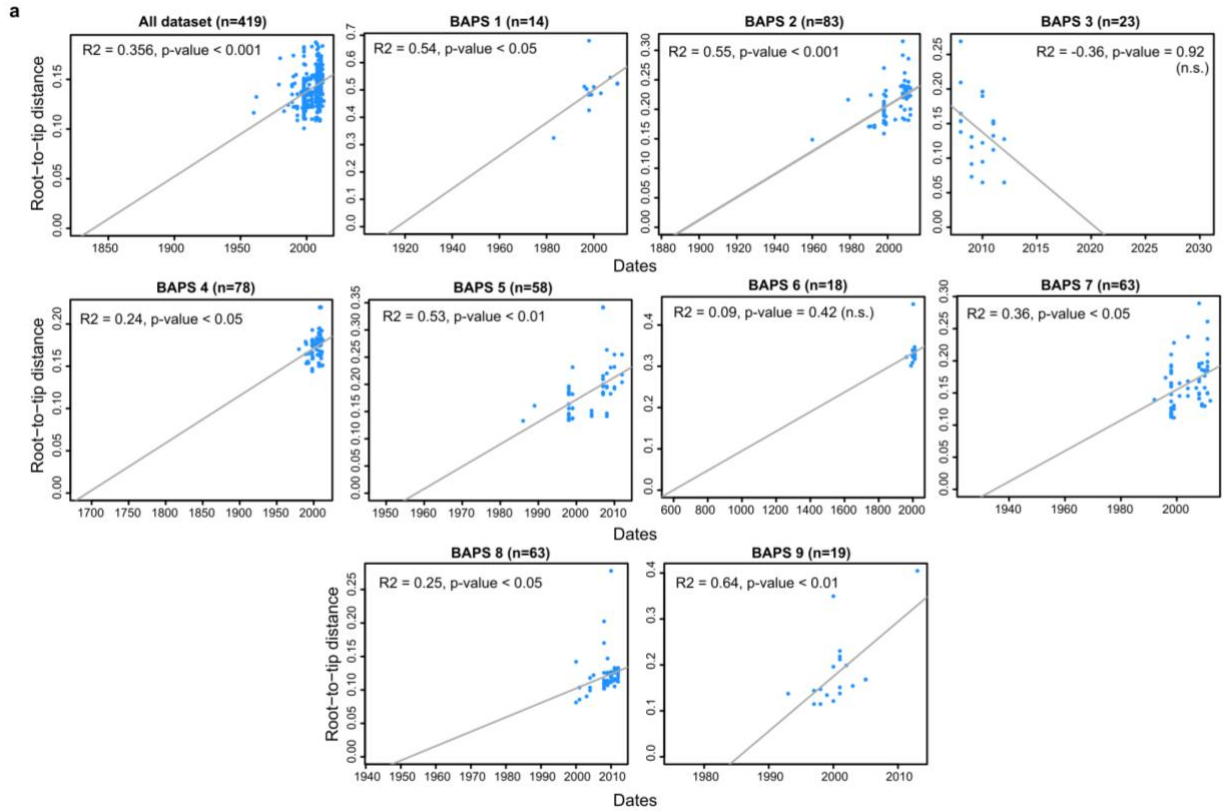
Supplementary Figures 1 to 10

Supplementary Tables 2, 3 and 5 to 7

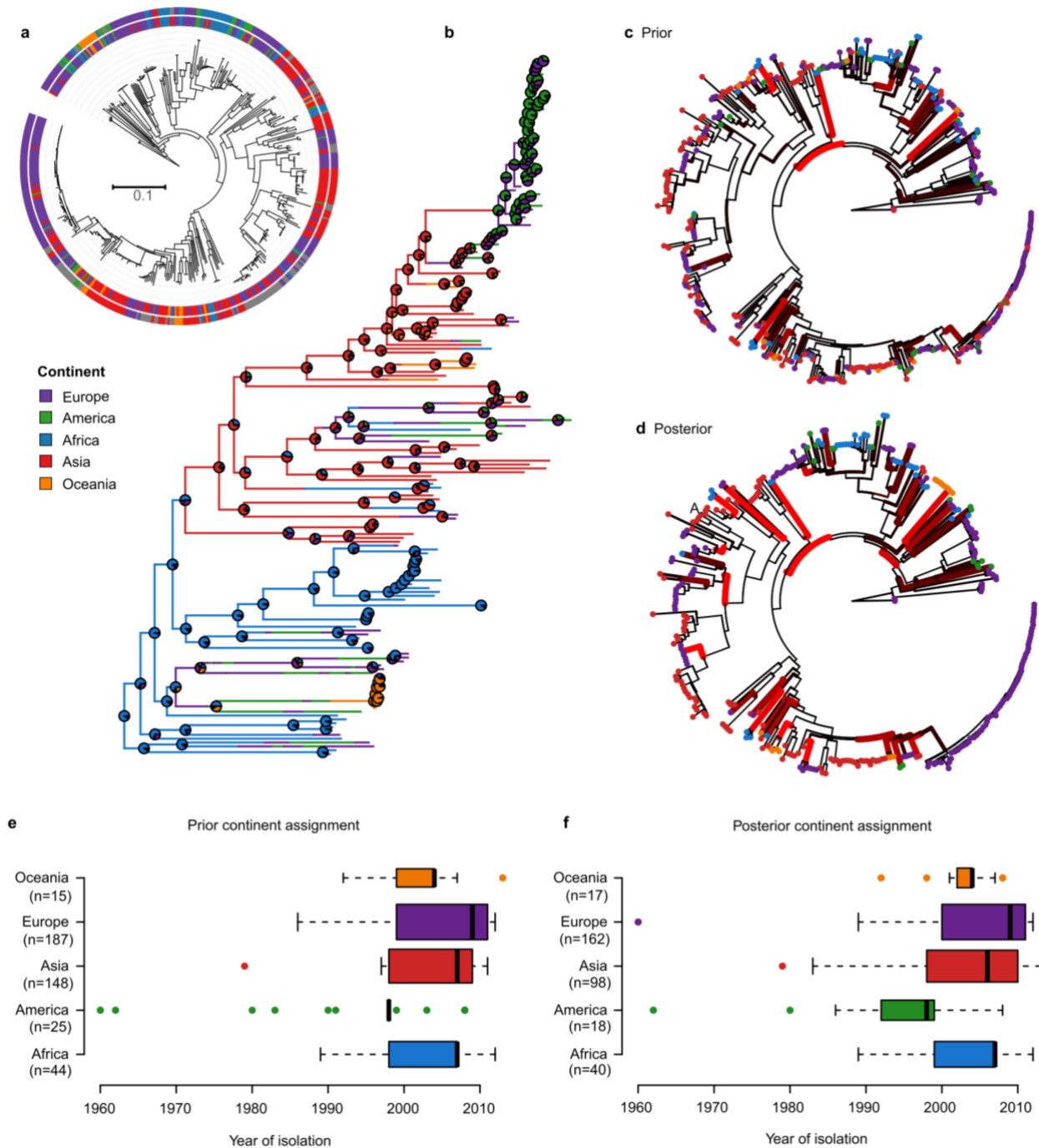
Supplementary Note



**Supplementary Figure 1 | Population structure analysis.** (a) Discriminant Analysis of Principal Components (DAPC) clustering of the *Neisseria gonorrhoeae* strains (n=419) by its continent of isolation (Wilk's lambda test p-value for discriminant function 1 < 0.0001, Supplementary Table 3) (b) Membership plot showing the posterior probability assignment of each strain to each of the continents. The bar above the plot shows the prior information on the continent of isolation per strain. (c) DAPC analysis of *N. gonorrhoeae* strains (n=419) with randomized continents showing no population differentiation by continent. (d) A-score optimization test performed to obtain the optimal number of principal components to retain in the DAPC analysis<sup>62</sup> as a trade-off between power of discrimination and over-fitting. Calculated as the difference between the proportion of successful reassignments and values obtained using random groups corrected by the number of retained components (<http://adegenet.r-forge.r-project.org/files/tutorial-dapc.pdf>).

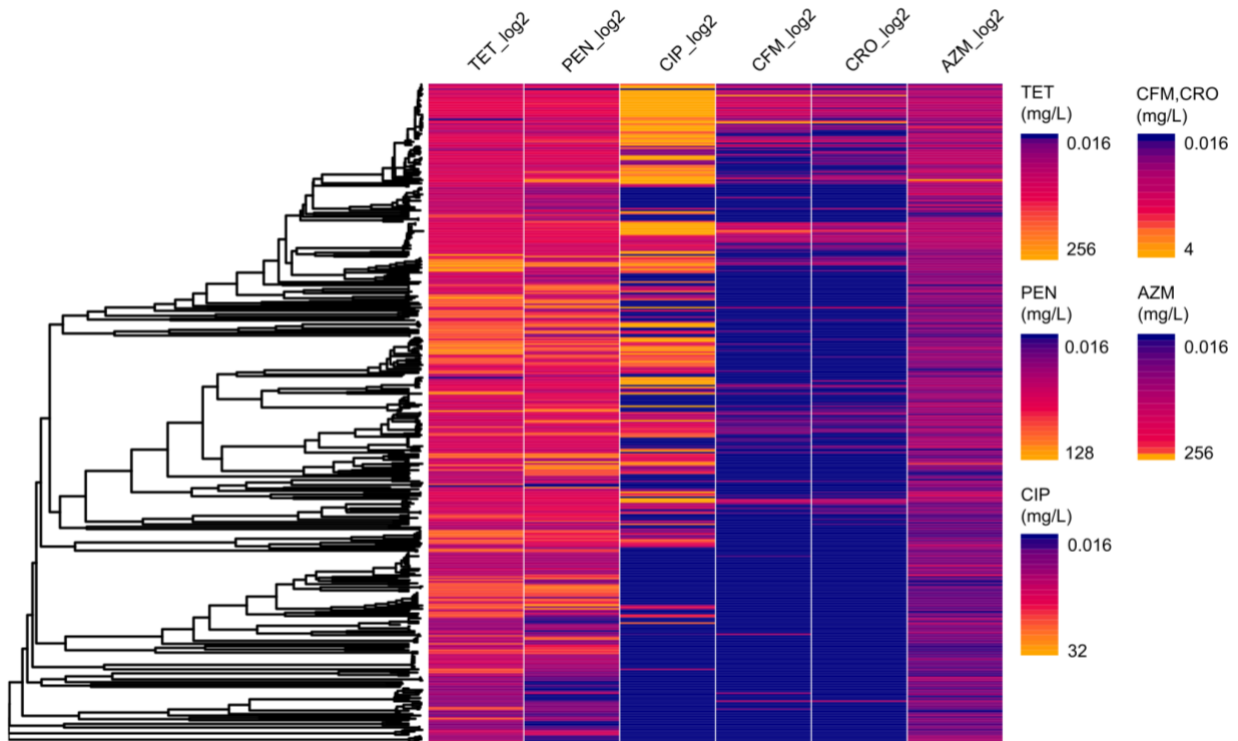


**Supplementary Figure 2 | Temporal signal, tMRCA and substitution rate estimation.** (a) Root-to-tip distance estimate over time of the 419 *N. gonorrhoeae* global collection (first plot) and the different BAPS clusters (following plots) calculated using a “clustered permutation” approach<sup>66</sup>. P-values for  $R^2$  were obtained by comparing the value of this coefficient obtained from the real data to those resulting from permuting the isolation dates (n=1000 permutations) as described in <sup>66</sup>. (b) Comparison between LSD<sup>68</sup> and BEAST<sup>69</sup>. Estimates of the tMRCA and the substitution rate for the five BAPS clusters that reached convergence in BEAST as well as the whole collection, calculated using BEAST and LSD. Blue segments represent the 95% HPD interval obtained for the tMRCA estimate in BEAST and orange segments represent LSD confidence intervals. Mean values are marked with a grey dot. (c) Distribution of the tree root height and substitution rate parameters estimated from two different BEAST chains after 100 million generations (burn-in=30 million). The 95% HPD interval from BEAST and the confidence interval obtained with LSD for the whole collection (n=419) are plotted below for comparison. n.s.=non-significant.

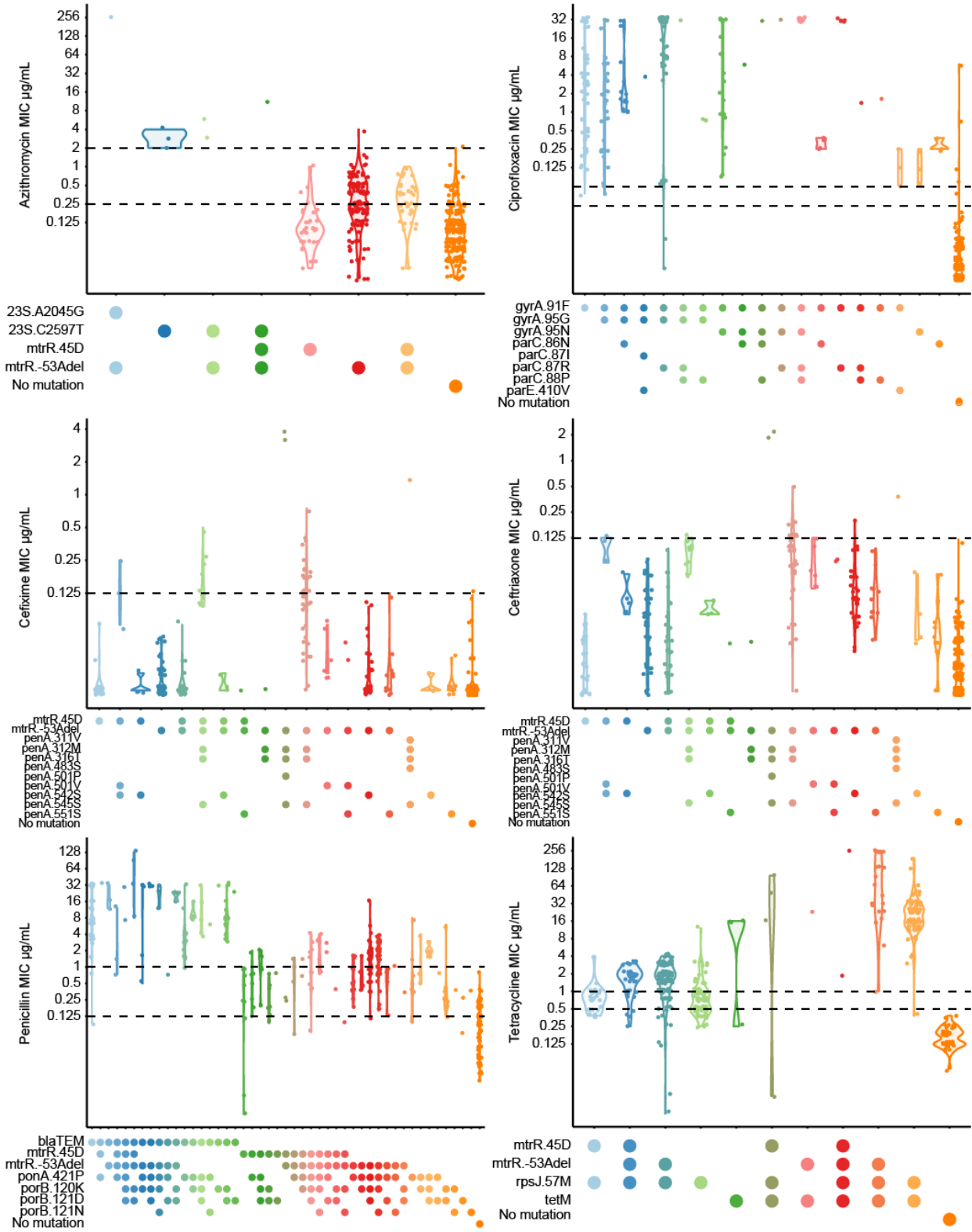


**Supplementary Figure 3 | Phylogeographic analysis.** (a) Maximum likelihood phylogenetic tree showing the tips ( $n=419$ ) coloured with the prior information on the continent of isolation (inner circle) and the posterior group membership after DAPC analysis<sup>62</sup> (outer circle). Admixed individuals are defined as those with  $<80\%$  posterior probability of assignment to any of the five continents and are shown in grey. (b) Stochastic mapping of the posterior continent assignments over the dated phylogenetic tree complemented with US strains from Grad *et al.* 2014<sup>16</sup> and using even number of strains from each continent ( $n=41$ ) except for

Oceania (n=17), for which there is not more available data in the public databases at the time of writing (total n=181). Analysis was performed using the *phytools* R package<sup>72</sup>. Pie charts in every node represent the proportion of ancestry to each of the five continents. (c-d) Per-branch posterior distribution of the trait “Continent” using both prior (c) and posterior (d) memberships along the phylogenetic tree calculated using *treeBreaker*<sup>70</sup>. (e-f) Distribution of isolation dates by continent shown for both prior (e) and posterior (f) continent assignments. Vertical box lines represent the first quartile, the median and the third quartile. Whiskers extend from the first quartile – 1.5x the interquartile range and the third quartile + 1.5x the interquartile range. The width of the boxplots is proportional to the number of strains from each continent (detailed in the figure).

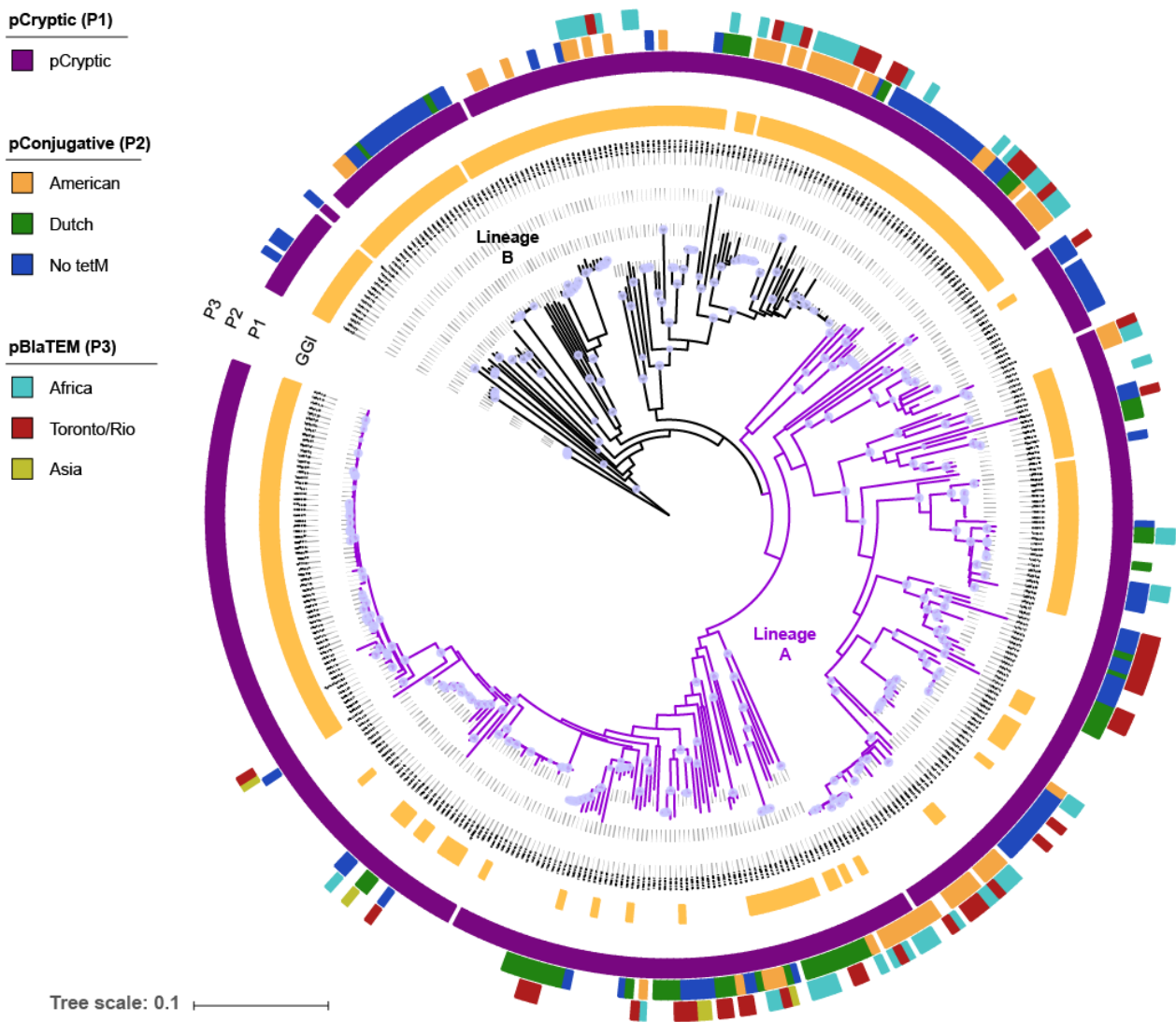


**Supplementary Figure 4 | Minimum Inhibitory Concentration (MIC, in mg/L) for six antimicrobials.** The distribution of the MICs of six antimicrobials is shown for all strains included in the analysis in log<sub>2</sub> scale. Note that the distribution of resistance is equivalent to that found from genotypic resistance. The scale of the cephalosporins CFM and CRO has been collided into one and the range of MICs in the legend is shown without logging. The minimum MIC value has been set to 0.016 mg/L for all antimicrobials. TET = Tetracycline, PEN = Penicillin G, CIP = Ciprofloxacin, CFM = Cefixime, CRO = Ceftriaxone, AZM = Azithromycin.



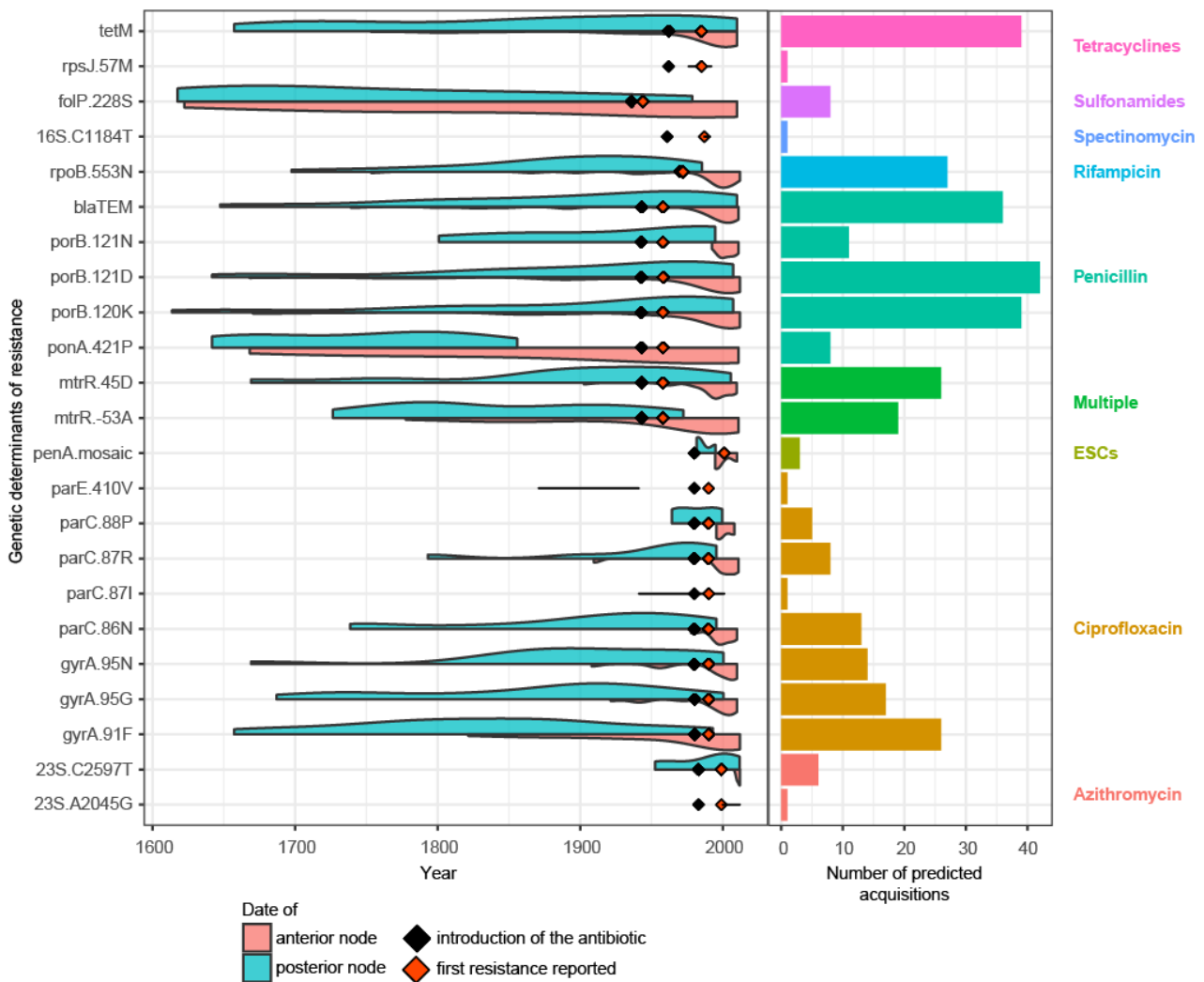


**Supplementary Figure 5 | Phenotypic and genotypic resistance.** Distribution of MIC values (in logarithmic scale) for each combination of antimicrobial determinants associated in the literature<sup>74</sup> to each of the six antimicrobials under study in the global gonococcal collection (n=419). Horizontal dashed lines mark EUCAST breakpoints ([www.eucast.org](http://www.eucast.org)) except for azithromycin, in which the CLSI 2 mg/L upper bound is also shown ([www.clsi.org](http://www.clsi.org)).

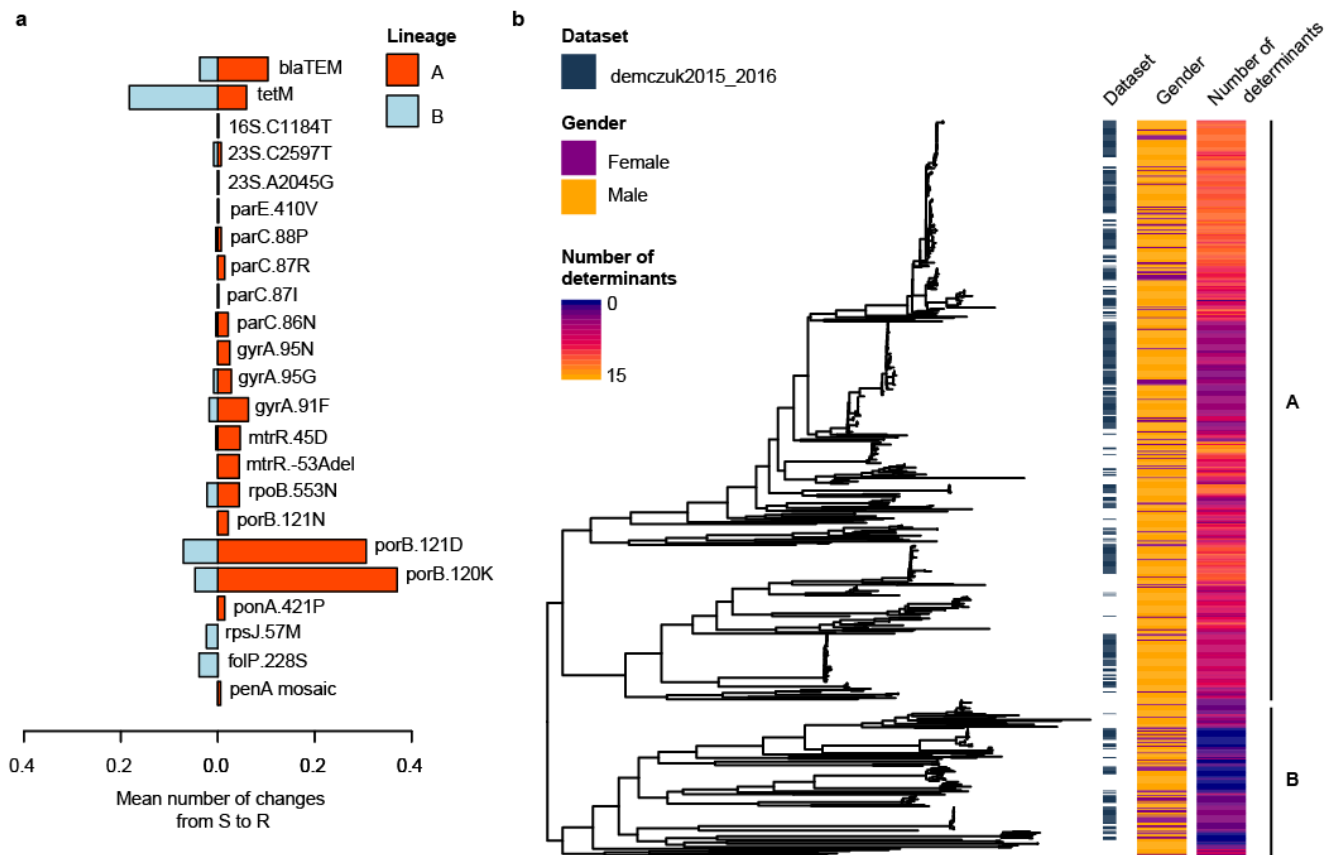


**Supplementary Figure 6 | Distribution of the Gonococcal Genomic Island and plasmids.**

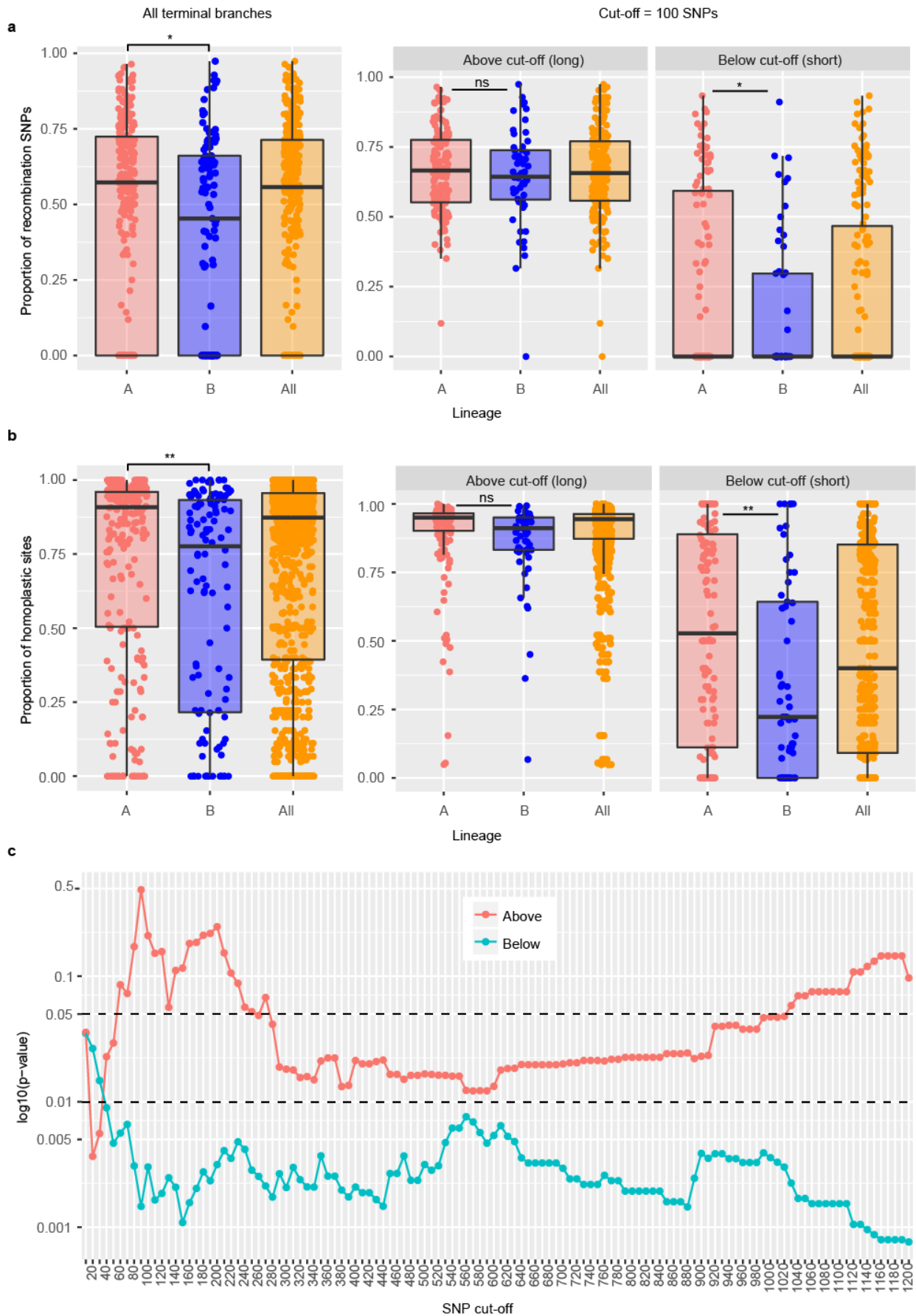
Maximum likelihood phylogenetic tree showing, from the inner to the outer circle: the occurrence of the Gonococcal Genomic Island (GGI) and the three main plasmids (pCryptic (P1), pConjugative (P2) and pBlaTEM (P3)). Colours in plasmid tracks correspond to different types, as described in the legend. The two lineages are marked in black (B) and purple (A), respectively. Node shapes represent bootstrap support values above 70%.



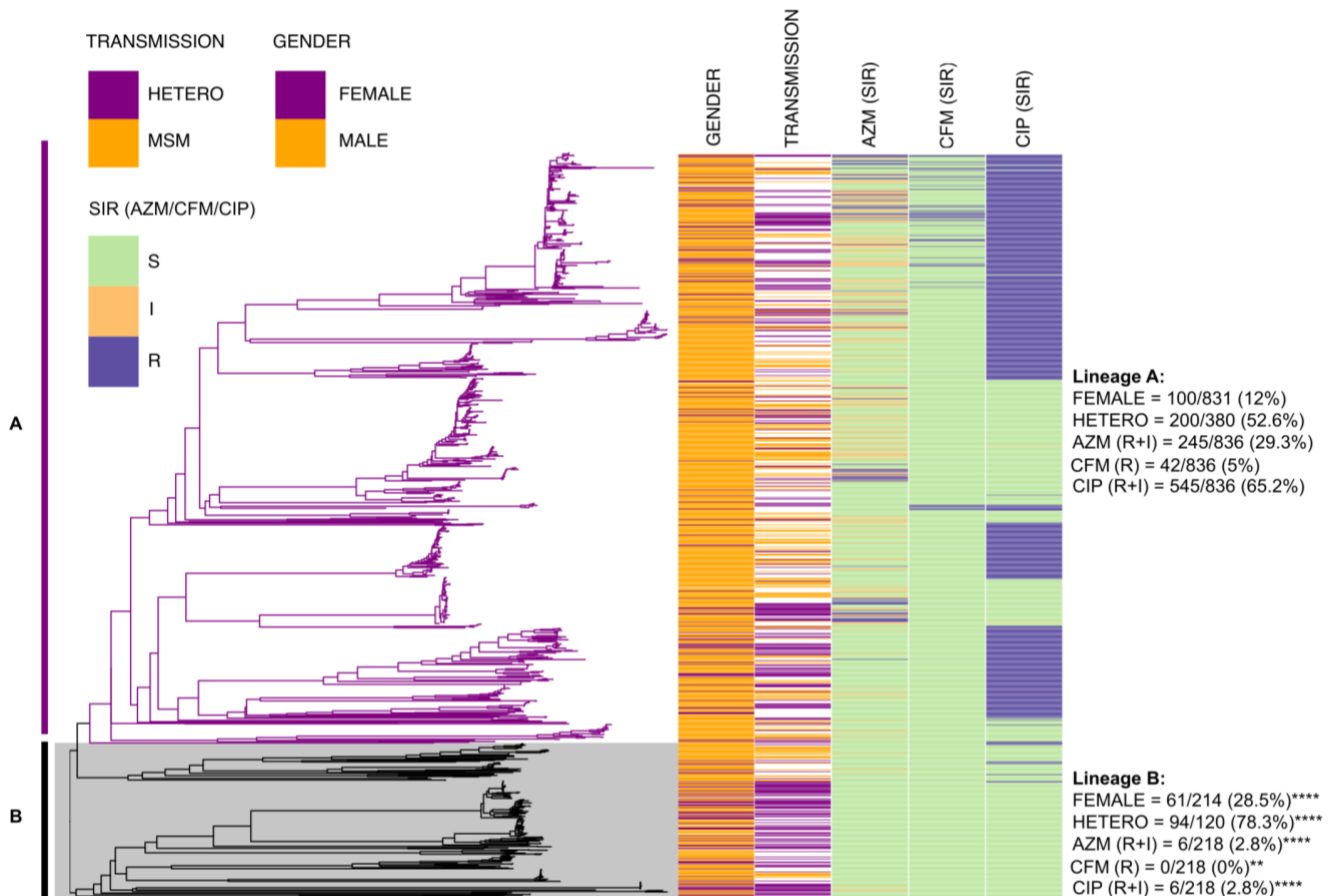
**Supplementary Figure 7 | Most predicted acquisitions of antimicrobial resistance happened after the introduction of antimicrobials.** The distribution of the predicted acquisitions of the known determinants of antimicrobial resistance along time are represented as half violin plots (pink when using the date of the anterior and blue the posterior nodes of the branch where the acquisition is predicted). Anterior and posterior nodes refer to those at the beginning and end of the branch, respectively. So, if a change happened in one branch, this would be accounted only if we look at the posterior nodes. The prediction was performed with ancestral maximum likelihood reconstruction (*ace* function of the *phytools* R package<sup>80</sup>) and a symmetric model of transition between states. Black diamonds mark the reported date of introduction of different antimicrobials to treat gonorrhoea and orange diamonds the first reported date of treatment failure. The barplot on the right shows the total number of predicted acquisitions for each mutation, and it is coloured to differentiate mutations affecting different antimicrobials.



**Supplementary Figure 8 | AMR genetic determinants in the two lineages.** (a) Mean number of changes from susceptible (S) to antimicrobial resistant (R) status inferred to have evolutionarily happened in lineages A and B for all the analysed resistance determinants, including the mosaic *penA*. Values have been corrected by the number of edges of the A (n=586) and B (n=236) subtree lineages, respectively. (b) Distribution of the patient's gender and the number of antimicrobial resistance determinants that the infecting strains carry. The figure shows a non-recombinant maximum likelihood tree of 639 strains (263 from the global collection and 376 from two North American studies<sup>17,26</sup>) with the mentioned information as metadata.



**Supplementary Figure 9 | Assessment of recombination SNPs and homoplastic sites in terminal branches.** (a) Proportion of SNPs inside the recombination events predicted by Gubbins for all terminal branches together and shorter ( $\leq 100$  SNPs) and longer ( $> 100$  SNPs) terminal branches separately in lineages A (n=298), B (n=121) and all strains (n=419). (b) Proportion of homoplastic sites in all terminal branches together and shorter ( $\leq 100$  SNPs) and longer ( $> 100$  SNPs) terminal branches separately lineages A, B and all strains. (c) Distribution of the p-values calculated using a two-sided Wilcoxon test on the number of homoplasies in the two lineages on short and long terminal branches of the tree at different SNP cut-offs. Significance thresholds at 0.01 and 0.05 are marked with a dashed line. Short branches are probably more reliable for this type of calculation than long branches and this can be observed at around a cut-off of 100 SNPs, where branches under this number of SNPs have a p-value  $< 0.005$  while the rest are clearly not significant p-value  $> 0.1$ . SNPs in repeat regions and those known to undergo antigenic variation, such as pilin-, opA54- or Maf-associated genes were excluded from the calculation. \*\*p-value  $< 0.01$ , \*p-value  $< 0.05$ , ns = non-significant.



**Supplementary Figure 10 | Pathogenwatch phylogenetic reconstruction of 1,054 strains from the Euro-GASP 2013 survey<sup>27</sup>.** The two lineages (A in purple, n=836, and B in black, n=218) were identified by combining this set with the global collection data as specified in the methods section. The metadata aligned to the tree shows the distribution of the gender of the patients from which the isolates were obtained, the type of transmission and the SIR categories of the phenotypic antimicrobial susceptibility test of the isolates following the breakpoints from EUCAST ([www.eucast.org](http://www.eucast.org)). Counts of each column are shown per lineage on the right side. Asterisks in lineage B indicate statistical significance compared to lineage A using a two-sided test for equality of proportions. AZM = Azithromycin, CFM = Cefixime, CIP = Ciprofloxacin. R = Resistant, I = Intermediate resistance, S = Susceptible. \*\*\*\*p-value<0.0001, \*\*p-value<0.01.

**Supplementary Table 1 | Additional strain information.** Metadata associated to the 419 *N. gonorrhoeae* strains included in the study, typing information and antimicrobial resistance determinants detected by ARIBA. Sex: M=Male, F=Female. Accessory: GGI=Gonococcal Genomic Island, pCryptic=cryptic plasmid, pBlaTEM=blaTEM plasmid, pConjugative=conjugative plasmid, isPCR=*in silico* PCR. Antibiotic resistance: B-LAC=Beta-lactamase, SPT=Spectinomycin, TET=Tetracycline, PENG=Penicillin G, CIP=Ciprofloxacin, CFM=Cefixime, CRO=Ceftriaxone, AZM=Azithromycin.

This table is provided as an external Excel file (Supplementary\_Table\_1.xlsx).

**Supplementary Table 2 | Analysis of Molecular Variance.** Analysis of Molecular Variance (AMOVA) calculated using three population levels: continent, subcontinent and country, for real and randomized population structure. Randomization shows no population structure at all, supporting the signal obtained by our data.

					Components of variance		
		Df	Sum Sq	Mean Sq	Sigma	%	p-value
Real population structure	Between continents	4	5973.115	1493.2789	7.458491	2.352675	0.947
	Between subcontinents within continent	19	14218.394	748.3365	16.152612	5.095112	0.01
	Between countries within subcontinent	34	13973.593	410.988	26.594308	8.388797	0.001
	Within countries	361	96320.685	266.8163	266.816302	84.163416	0.001
	Total	418	130485.788	312.167	317.021712	100	-
Randomization of population	Between continents	4	1562.217	390.5543	1.18256	0.3783702	0.938
	Between subcontinents within continent	19	5892.563	310.1349	-1.373468	-0.439453	0.463
	Between countries within subcontinent	34	10988.096	323.1793	2.363171	0.7561169	0.369
	Within countries	361	112042.912	310.3682	310.368177	99.3049659	0.135
	Total	418	130485.788	312.167	312.54044	100	-



**Supplementary Table 3 | Multivariate Analysis of Variance.** Results of the Multivariate Analysis of Variance (MANOVA, Wilk's lambda test) calculated to assess the significance of each discriminant function in the DAPC analysis. \*\*\*\*p-value<0.0001.

	<b>Df</b>	<b>Sum Sq</b>	<b>Mean Sq</b>	<b>F value</b>	<b>Pr(&gt;F)</b>	
<b>LD1</b>	4	1624.90162	406.225405	406.225405	7.84E-142	****
<b>LD2</b>	4	435.5227276	108.8806819	108.8806819	2.57E-63	****
<b>LD3</b>	4	225.1793729	56.29484322	56.29484322	6.67E-38	****
<b>LD4</b>	4	216.2578294	54.06445735	54.06445735	1.19E-36	****
<b>Residuals</b>	414	414	1			

**Supplementary Table 4 | Prior and posterior continent assignments.** Prior and posterior assignments to continents for each of the strains included in the study after running a DAPC analysis.

This table is provided as an external Excel file (Supplementary\_Table\_4.xlsx).

**Supplementary Table 5 | Membership assignments by continent.** Number of prior and posterior membership assignments to each continent after DAPC analysis.

		Posterior						Total	% admixture detected	% assigned to another continent
		Admixture	Africa	America	Asia	Europe	Oceania			
Prior	Africa	5	36	2	1	0	0	44	11.36	6.82
	America	6	0	11	1	7	0	25	24.00	32.00
	Asia	36	2	2	87	19	2	148	24.32	16.89
	Europe	34	2	3	7	135	6	187	18.18	9.63
	Oceania	3	0	0	2	1	9	15	20.00	20.00
	Total	84	40	18	98	162	17	419	20.05	13.60

**Supplementary Table 6 | Root ancestry.** Percentage of ancestry of the root node of the tree to each of the five continents (posterior assignments). Summary of 1000 stochastic maps. The analysis was repeated by incorporating extra American strains from Grad *et al* 2014<sup>16</sup>. The number of strains with a posterior assignment to each continent used in each analysis is specified between brackets. Even sampling was obtained by subsampling the strains from different continents 100 times and performing 10 stochastic maps on each of them. Continents were randomised on an evenly sampled tree including extra American strains and the analysis repeated using 1000 stochastic maps. The highest percentage is highlighted.

	<b>Africa</b>	<b>America</b>	<b>Asia</b>	<b>Europe</b>	<b>Oceania</b>
<b>Global collection</b>	31.3% (N=40)	7.7% (N=18)	0.1% (N=98)	60.9% (N=162)	0% (N=17)
<b>Global collection and Grad <i>et al</i> 2014</b>	33.2% (N=41)	42.2% (N=237)	0.2% (N=108)	24.4% (N=186)	0% (N=17)
<b>Global collection and Grad <i>et al</i> 2014 (down sampling)</b>	90.7% (N=41)	2.1% (N=41)	0.8% (N=41)	6.4% (N=41)	0% (N=17)
<b>Random continents</b>	20.3% (N=41)	18.2% (N=41)	22.5% (N=41)	20.1% (N=41)	18.9% (N=17)

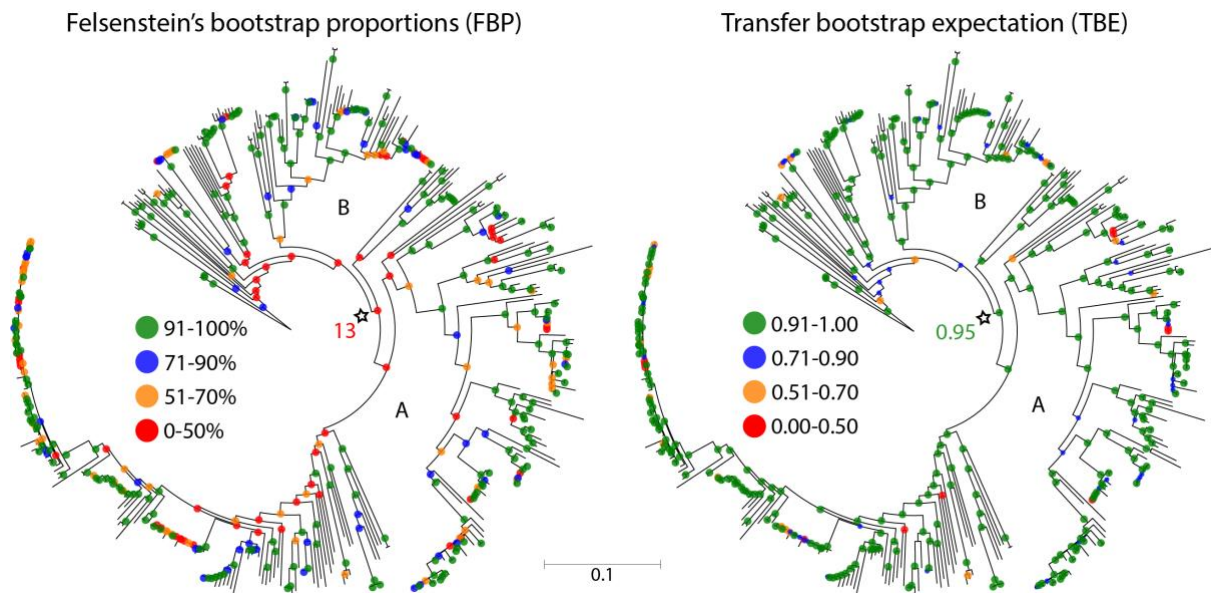
**Supplementary Table 7 | Estimates of the substitution rate and tMRCA from BEAST and LSD.** Estimates of substitution rate and time for the Most Recent Common Ancestor (tMRCA) for five BAPS clusters obtained with BEAST and LSD. R<sup>2</sup> shows the correlation coefficient between the root-to-tip distances and dates of isolation. HPD = High Posterior Density.

		BAPS_1	BAPS_2	BAPS_5	BAPS_8	BAPS_9	All
	<b>Number of strains</b>	14	83	58	63	19	419
	<b>Number of SNPs</b>	1521	5239	4540	1174	316	15562
	<b>R<sup>2</sup></b>	0.54	0.55	0.53	0.25	0.64	0.36
	<b>(p-value)</b>	* < 0.05	*** < 0.001	** < 0.01	* < 0.05	** < 0.01	*** < 0.001
<b>BEAST</b>	<b>tMRCA</b>	1896.1806	1825.5614	1891.31	1972.3513	1985.5699	1575.0439
	<b>95% HPD int.</b>	[1861.87 - 1925.22]	[1807.75 - 1842.87]	[1875.75 - 1905.45]	[1964.43 - 1979.68]	[1981.84 - 1989.08]	[1549.64 - 1598.71]
	<b>Substitution rate (s/s/y)</b>	2.83E-06	4.13E-06	5.17E-06	2.94E-06	2.88E-06	4.66E-06
	<b>95% HPD int.</b>	[2.00E-06 - 3.65E-06]	[3.73E-06 - 4.56E-06]	[4.48E-06 - 5.81E-06]	[2.39E-06 - 3.52E-06]	[2.29E-06 - 3.44E-06]	[4.39E-06 - 4.91E-06]
<b>LSD</b>	<b>tMRCA</b>	1940.58	1807.95	1808.97	1961.01	1981.52	1589.0436
	<b>Confidence interval</b>	[1928.33 - 1948.69]	[1786.117 - 1826.523]	[1752.948 - 1840.652]	[1946.809 - 1970.174]	[1975.303 - 1985.155]	[1544.25 - 1622.99]
	<b>Substitution rate (s/s/y)</b>	5.90E-06	4.41E-06	3.07E-06	2.38E-06	2.56E-06	3.74E-06
	<b>Confidence interval</b>	[4.89E-06 - 6.80E-06]	[3.95E-06 - 4.87E-06]	[2.41E-06 - 3.64E-06]	[1.86E-06 - 2.97E-06]	[2.01E-06 - 3.13E-06]	[3.39E-06 - 4.07E-06]

## Supplementary Note

### *Felsenstein's Bootstrap Proportions (FBP) vs Transfer Bootstrap Expectation (TBE)*

Felsenstein's Bootstrap Proportions (FBP) have been widely used to get support values for nodes in phylogenetic trees. However, a recent study suggests another methodology, called Transfer Bootstrap Expectation (TBE), implemented in BOOSTER<sup>56</sup>, which can be used for large datasets. In FBP, a branch must match exactly that in the original tree in each bootstrap replicate in order to be accounted for the support value, producing lower values than expected. In TBE, a transfer distance is calculated to the original branch, resulting in higher support values, specially at the deeper nodes. We have used both methodologies to estimate node values in the maximum likelihood phylogenetic tree of the strains included in this study, and show that FBP generates support values for the ancestral nodes between 0 and 50%, while the TBE values for the same nodes using BOOSTER are  $>0.90$ . The node that marks the split between lineage A and B is marked with a star.



### ***Bayesian phylogenetic inference using BEAST***

Bayesian inference was attempted with BEAST<sup>39</sup> to estimate the substitution rate of *N. gonorrhoeae* and the time of the Most Recent Common Ancestor (tMRCA) of the whole set of strains under study. Significant temporal signal was found ( $R^2 = 0.36$ ,  $p$ -value  $< 0.001$ ; Supplementary Figure 2) after estimating the root-to-tip distance correlation over time. However, obtaining good mixing in BEAST for datasets as large and complex as this one (419 strains with 15,562 SNPs) can be troublesome, especially for highly diverse bacterial populations. Recombination was removed from the dataset as one of the first steps, however, a considerable number of homoplastic sites in internal branches remained and these could have an effect in the mixing capacity of a Bayesian MCMC approach.

In order to simplify the problem, hierBAPS<sup>55</sup> was run on the dataset to obtain genetically uniform clusters. Nine groups were detected (Figure 1), most of which were monophyletic except for clusters 4 and 7. Genetic and temporal correlations were evaluated for all clusters, but only seven showed a significant temporal signal (Supplementary Figure 2). Five of those showed MCMC convergence using BEAST (Supplementary Table 7), which revealed an average substitution rate of  $3.43E-06$  substitutions per site per year (s/s/y) (95% HPD interval [ $2.98E-06 - 4.20E-06$  s/s/y]). The estimated tMRCAs ranged from 1825.6 (95% HPD interval [ $1807.8 - 1842.9$ ]) in BAPS\_2 to 1985.6 (95% HPD interval [ $1981.8 - 1989.1$ ]) in BAPS\_9.

### ***Comparison between BEAST and LSD estimates***

To confirm that the estimates from LSD were reliable, it was run on the five BAPS clusters with good mixing in BEAST (BAPS clusters 1, 2, 5, 8 and 9) and the estimates from the two methods were compared. Results from both programs were compatible, within the same order of magnitude and with mostly overlapping confidence intervals (Supplementary Figure 2 and Supplementary Table 7). Despite not reaching acceptable convergence in all the parameters, two BEAST chains were run for 100 million generations on the whole collection. The distribution of the tree root height parameter on both runs after removing the burn-in was completely overlapping with the LSD estimates and rate estimates were of the same order of magnitude (Supplementary Figure 2).

### *Statistical testing of the obtained tMRCA*

To corroborate the tMRCA obtained by LSD<sup>38</sup>, the software was run multiple times by fixing the date of the node leading to the main introduction to Asia in the early 17<sup>th</sup> century at above 1500 different time points between year 0 and 1959. To test a hypothesis about the date of a node against the LSD estimate, we used the Wald statistic<sup>81</sup>, which is generally used for testing point null hypotheses with approximate log-likelihood functions that can be calculated numerically. The test statistic equals the squared distance between the parameter value according to the null hypothesis and the approximate maximum likelihood estimate (MLE), multiplied by the curvature of the log-likelihood function at the MLE. The curvature is measured by the second derivative of the function. To obtain an accurate numerical approximation, we fitted a second-degree polynomial to the log-likelihood function around the MLE, which indicated a close fit of a quadratic function with mean squared error equal to 7.06E-06. The Wald statistic is asymptotically distributed according to the Chi<sup>2</sup>-distribution with a single degree of freedom for one restricted parameter, which is used to calculate the p-value of any particular date. Results revealed a single optimal value between 1622 and 1623, close to year 1622.3, estimated by LSD in the target node as the inferred year of introduction to Asia.

Furthermore, LSD was run several times with the root fixed at dates ranging from 10,000 years Before Common Era (BCE) to the 20<sup>th</sup> century and the obtained substitution rates and objective functions evaluated. Results showed that if the emergence of this collection had been between 10,000 BCE and year 0, the corresponding substitution rate for the species would have been at least one order of magnitude slower than previous reports. Contrarily, if the emergence had been more recent (i.e. 20<sup>th</sup> century) the substitution rate would have been at least one order of magnitude faster.

81 Casella, G. & Berger, R. L. *Statistical inference (Vol. 2)*. (Pacific Grove, CA: Duxbury, 2002).